A Multiband Model With Successive Projections Algorithm for Bathymetry Estimation Based on Remotely Sensed Hyperspectral Data in Qinghai Lake

Dianjun Zhang, Quan Guo, Lingjuan Cao, Guoqing Zhou, *Senior Member, IEEE*, Guangyun Zhang, and Jie Zhan

***Abstract*—Lake bathymetry plays a pivotal role in environmental monitoring, ecological management, water quality protection, etc. Hyperspectral remote sensing technology can provide large-scale coverage and more detailed spectral information for bathymetry estimation than traditional measurements or multispectral imagery techniques. In this study, a multiband linear model with successive projections algorithm (SPA-MLM) was developed to retrieve the bathymetry of Qinghai Lake, which is the largest inland saltwater lake in China. The three most sensitive spectral bands were first selected by the SPA, and a multiband linear model was established by the least squares method combined with the *in situ* measured water depth. Zhuhai-1 hyperspectral remotely sensed imagery is employed as the data source. In all, 98 *in situ* bathymetry measurements matched with the obtained images were obtained during three surveys performed in May, September, and October 2020. The results demonstrated that the established retrieval model can be used to accurately estimate the water depth in the study area, with an accuracy exceeding approximately 90%, which suggests that the proposed model performs better than those used in previous studies employing hyperspectral imagery. The correlation coefficient reaches 0.92, and the root-mean-square error is approximately 1.26 m. This demonstrates that bathymetry estimation obtained using remotely sensed hyperspectral data is an effective detection method and can provide large-scale, rapid monitoring data to the relevant decision-making departments.**

***Index Terms*—Bathymetry, hyperspectral remote sensing, multiband model, successive projections algorithm (SPA).**

I. Introduction

LAKE bathymetry can provide fundamental modeling parameters and act as a basis for scientific research and government decision-making; it is an important component of lake environmental monitoring, water quality management, sustainable utilization development, and engineering construction planning [1]–[6]. Satellite-based bathymetry has been continuously developed over several years utilizing the promising advantages of remote sensing; however, traditional measurement methods cannot be implemented in parallel. The large-scale coverage achieved utilizing the synchronous observation capabilities and fast detection scheme of remotely sensed technology, which even enables the collection of long time series observations, presents another solution for the economical estimation of water depth. It has gradually become a common technique for bathymetry methods implemented in lake and ocean studies.

Satellite-based bathymetry technology mainly includes multispectral scanners and microwave synthetic aperture radars (SARs) as well as high spectrometers [7]–[10]. Simplified or empirical algorithms are used to retrieve water depth from multispectral data under clear-sky conditions, which have a low accuracy and require conventional bathymetric data to calibrate model parameters. The retrieval of shallow water depth through all-weather SAR images also requires the calibration of bathymetric data, which is influenced by surface wind fields. The retrieval of shallow water depths with clear sky hyperspectral data does not depend on conventional water depth data. High retrieval precision can be achieved, and the submarine reflectivity and inherent optical parameters of seawater can be obtained synchronously. Compared with SAR methods, although satellite hyperspectral data are limited by atmospheric conditions, lake water depth is considered an environmental parameter that changes slowly. Therefore, the emergence of hyperspectral sensors has improved the spectral resolution and is conducive to identifying water information with weak reflected signals for lake bathymetry in complex environments [11]–[13].

On the basis of sufficient spectral information, hyperspectral remote sensing has the characteristics of "map integration," which can be used to obtain the spatial and spectral information of the ground features. Since the 1980s, with the increasing enrichment of hyperspectral data, the water depth retrieval model has been heavily developed, and various forms have been proposed [5], [14]–[18], such as follows:

1) the look-up table method;
2) the spectral differential statistical model;
3) the neural network model;
4) the semianalytical model.

Manuscript received April 10, 2021; revised June 19, 2021; accepted June 27, 2021. Date of publication June 30, 2021; date of current version July 20, 2021. This work was supported in part by the National Key R&D Program of China under Grant 2018YFC1407400 and in part by the National Natural Science Foundation of China under Grant 42001274. *(Corresponding author: Dianjun Zhang.)*

Dianjun Zhang, Quan Guo, Lingjuan Cao, and Jie Zhan are with the School of Marine Science and Technology, Tianjin University, Tianjin 300072, China (e-mail: zhangdianjun123@163.com; gq341300@tju.edu.cn; 2020227020@tju.edu.cn; zhanjie_2019@tju.edu.cn).

Guoqing Zhou is with the Guangxi Key Laboratory for Spatial Information and Geomatics, Guilin University of Technology, Guilin 541004, China (e-mail: gzhou@glut.edu.cn).

Guangyun Zhang is with the School of Geomatics Science and Technology, Nanjing Tech University, Nanjing 211816, China (e-mail: gyzhang1234@163.com).

Digital Object Identifier 10.1109/JSTARS.2021.3093624

According to previous studies, the depth estimate produced by water depth retrieval is more accurate than many multispectral-based methods [18]. The look-up table method aims to establish a remote sensing reflectance spectrum library for the study area through model simulation [19]. The remote sensing reflectance extracted by the hyperspectral image through atmospheric correction was compared with the spectrum library. The detection results were obtained by taking the water depth corresponding to the most closely matched spectrum. This model considers robust ocean optical theory and requires detailed numerical simulation, and the simulations in detail should consider the optical components and water characteristics in the study area to ensure the accuracy of water depth inversion. Mobley *et al.* [20] established a remote sensing reflectance spectrum database based on the hydrolight radiation transmission model, used the least squares method to match the reflectivity of an image to a database, and extracted the water depth of the matched spectrum. The result was compared with sonar sounding data, and the average error was 0.5 m. Zhang *et al.* [21] developed a remote sensing reflectance spectrum library through a radiation transmission model and applied the look-up table and spectrum matching method to extract underwater topography from hyperspectral airborne, visible, infrared, imaging spectrometer (AVIRIS) imagery of Peter Island in the Virgin Islands. The test results showed that rapid water depth detection in coastal areas is feasible using calibrated hyperspectral imagery. The spectral differential model establishes the statistical relationship between the derived parameters of the spectrum and the water depth through regression analysis [22]. Previous research results showed that the inversion accuracy of the spectral differential model is better than that of the single-band model and the spectral band ratio model, especially for water bodies with high turbidity near the shore [23]. The advantages are more obvious, and there are examples showing that the average relative error of the differential model is less than 17% [24]. Spectral differentiation technology can remove portions of the background noise's influence on the target spectrum and reduce the influence of water turbidity changes on the inversion of water depth. However, the statistical differential spectral model uses very little band information in the hyperspectral data, and it is difficult to take advantage of the abundant bands provided by hyperspectral remote sensing due to its model mechanism. The neural network model is suitable not only for multispectral water depth inversion but also for hyperspectral water depth inversion. Sandidge and Holyer [25] applied neural network models and AVIRIS aerial hyperspectral remote sensing imagery to invert the water depth along the west coast of Florida and the Florida Keys, and the results showed that the root-mean-square error (RMSE) was 0.84 and 0.39 m at water depths of 0–6 m. Shi [26] performed principal component analysis on input simulated hyperspectral data to improve the learning speed of the neural network. The simulated data are inverted by shallow sea depth through the established three-layer artificial neural network model, and the inversion result is better than the semianalytical model. On the basis of classifying the bottom material of the seafloor, Grigorieva proposed a method for multispectral and hyperspectral water depth inversion using an artificial neural algorithm. The experiment verified that the relative error of the sounding was approximately 14%. The hyperspectral optimization process exemplar (HOPE) model is currently the most influential and widely used hyperspectral water depth inversion model for remote sensing data. This model was proposed by Lee *et al.* [10] in 1999 and performs the joint inversion of shallow seawater depth and inherent optical properties. The model fully considers the absorption and scattering factors of water components, and the physical mechanism is relatively complete. Its greatest advantage is that the water depth does not need to be measured, and it can directly perform water depth inversion. Therefore, it has been favored by many scholars worldwide, and a large number of studies have been carried out with it. The accuracy of the research results is generally high. The average relative error is approximately 15% within the 0–25 m water depth range. In 2001, Lee *et al.* [27] used the HOPE algorithm and AVIRIS hyperspectral data to obtain the water depth, seabed reflectance, water volume absorption coefficient, and water backscattering coefficient. In 2007, Lee *et al.* used the HOPE algorithm and Hyperion data to retrieve the shallow water depth and inherent optical properties in the Florida Keys. The water depth retrieval results were compared with LIDAR sounding data, and the relative error was approximately 11% [28].

Using remotely sensed hyperspectral data for bathymetry estimation, the first task is to select the characteristic bands that are sensitive to water depth, i.e., feature band extraction. Many approaches have been developed to select the appropriate feature bands, such as the regression coefficient method, x-loading weights method, independent component analysis (ICA) method, and successive projections algorithm (SPA) [29]. The regression coefficients are obtained during the partial least squares modeling process [30], [31]. The magnitude of the regression coefficient corresponding to each wavelength point indicates the impact of the wavelength on the model prediction performance. Therefore, the characteristic wavelength can be extracted according to the absolute value of the wavelength regression coefficient. The x-loading weights method is also performed during the partial least squares modeling process [32], [33], and the loading factor corresponding to each wavelength point can be obtained under each hidden variable. The absolute value of the load coefficient indicates the influence of the wavelength on the predicted performance of the established model. Therefore, the characteristic wavelength can be extracted according to the absolute value of the load coefficient under a certain implicit variable. The number of extracted characteristic wavelengths is generally the same as the number of hidden variables required for modeling, and one wavelength for each hidden variable is selected. One wavelength (the corresponding maximum absolute value of the load factor) is used as the characteristic wavelength. ICA is a new signal processing technique developed to address the problem of blind signal separation [34], [35]. ICA mainly uses non-Gaussian signals as the research object. Under the assumption of independence, it performs blind source separation of multichannel observation signals. It is mainly used in feature extraction, image processing, image compression, biomedical signal processing and analysis, finance, etc. [36]. In terms of spectral analysis, there have been

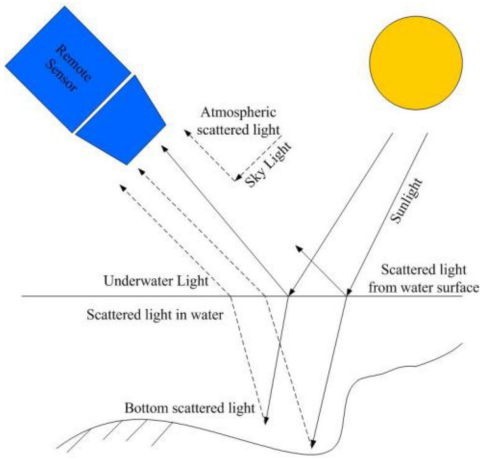

Fig. 1. Energy transmission process received by the sensor.

many related application studies [37]. The basic idea of the SPA is to find the variable group containing the minimal amount of redundant information in the spectral matrix to minimize the collinearity between the variables. The characteristic wavelength extracted by the SPA has the lowest redundancy and the least collinearity. The wavelength extracted by the SPA can represent the spectral information of most samples, thereby avoiding information overlap to the greatest extent [38], [39]. In this study, SPA is applied to retrieve the sensitive bands, and a multiband model is proposed for bathymetry estimation in Qinghai Lake. The Zhuhai-1 hyperspectral remotely sensed images are chosen as the data source that has never been used before in previous studies on bathymetry retrieval.

II. Methodology

A. Physical Basis of Remote Sensing Water Depth Inversion

The optical satellite-based methods used for bathymetry estimation depend on the characteristics of the water-reflected radiation entering the sensors, which is influenced by environmental factors when the radiation is transmitted in the atmosphere. An overview of the transmission path is depicted in Fig. 1. Light penetrates the atmosphere and reaches the water surface, and a portion of the energy is reflected at the air-water interface. Most of the energy is refracted by the water surface and enters the water body. Due to the absorption and scattering characteristics of the water body, the light waves continue to attenuate during the propagation process. At the same time, a portion of the scattered light will be reflected in the air, and a small portion of the light will reach the bottom. After reflection from the bottom, it will also return to the air and be received by the sensor through the atmosphere.

As shown in Fig. 1, the radiation energy received by the sensor can be expressed as

$$L_s = L_T + L_P \tag{1}$$

where L_S is the radiation received by the sensor, L_T refers to the target radiation after atmospheric transmission, and L_P represents the atmospheric path radiation (backscatter).

The water depth information is included in the L_T calculation, which can be parameterized as

$$L_T = (L_E + L_{\mathrm{ws}})T_\varphi = (R_E + R_{\mathrm{ws}})T_\varphi I \tag{2}$$

$$I = E_0 T_\theta \cos\theta + E_D \tag{3}$$

where L_E is the water-leaving radiation; L_{ws} represents the water surface radiation; T_φ is the atmospheric transmittance; R_E and R_{ws} are the water effective reflectivity and water surface reflectivity, respectively; E_0 is the solar irradiance outside the atmosphere; and E_D is the diffusive sky illuminance

$$L_E = f_1(L_b, L_w) \tag{4}$$

where L_b and L_w are the underwater radiation and backscattered radiation of the material in the water

$$L_T = f_2(T_\varphi, L_b, L_w, L_{ws}). \tag{5}$$

L_T mainly contains the following three kinds of water body information.

1) The radiation energy directly reflected by the surface of the water body, L_{ws}.
2) The backscattered radiation energy of the water body, L_w.
3) The underwater reflected radiation energy, L_b.

The amount of light information directly reflected by the surface of the water body is related to the water surface condition, which reveals no information regarding the waterdepth. Regardless of the atmospheric effect, if the water body is clear and shallow, the amount of light information received by the sensor is mainly related to the water depth. The reduction factor is related to the reflectivity of the water body. If the water contains suspended substances or other substances that can scatter light signals, the signal received by the sensor is related to the concentration of these substances and other abovementioned analyzed factors.

B. Hyperspectral Remote Sensing Images Preprocessing

Although ideal remote sensing images can truly reflect the radiation energy distribution and geometric characteristics of underlying surface conditions without distortion, they are affected by many factors, such as sensors, atmosphere, remote sensing platforms, and surface heterogeneity, in the process of satellite-based information transmission, receiving, and processing, resulting in the geometric deformation and radiation distortion of remote sensing images. It is necessary to correct these distortions to reflect the true features of the objects. The data are generated after a series of processing steps, including speckle removal, background removal, echo correction, radiometric correction, bad pixel recovery, and remote sensing image quality inspection. There are still many poor-quality bands or bands containing "abnormal pixels." Therefore, it is necessary to preprocess hyperspectral remote sensing images to restore them before using remote sensing images.

In this study, remote sensing image preprocessing mainly includes radiometric calibration, atmospheric correction, geometric correction, image mosaicking, and clipping. Radiometric calibration is the process of converting the measured value obtained by the sensor into absolute brightness or relative values

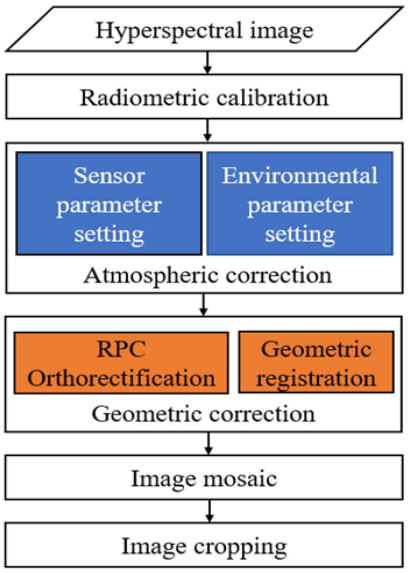

Fig. 2. Flowchart for hyperspectral data preprocessing.

related to physical quantities such as surface reflectivity and surface temperature. This process was conducted under ENVI software using the calibration coefficient that is provided in the image header file. Atmospheric radiometric correction can reduce or eliminate the image information distortion caused by clouds and water vapor. ENVI software was used for remote sensing image preprocessing, and the selected atmospheric correction model was FLAASH. After atmospheric radiometric correction, the spectral reflectance curves were checked, and the image reflectance was normalized. Geometric precision correction can reduce the geometric position difference between images. In all, 20 ground control points collected by high-precision GPS were applied to the image geometric correction. The second-order polynomial equation was used and the nearest neighbor method was chosen for the pixel value sampling with the accuracy of 1 pixel. The image data located in the study area were obtained by mosaicing and clipping. The overall preprocessing flowchart is described in Fig. 2.

C. Successive Projections Algorithm

The SPA determines the variable group with the least redundant information resulting from the spectral variables, and the collinearity among the variables in the group is minimized [40]. The principle of the algorithm is to construct new variables by projecting and mapping the spectral data and evaluate the new variable prediction effect based on multiple linear regression. The SPA only selects a few columns of the original spectral data, but it can summarize the spectral variable information of most samples, thereby avoiding the duplication of redundant information to the greatest extent. It greatly reduces the number of variables in the process of model establishment and improves the accuracy and performance of the model. The description of the algorithm is as follows [41].

1) Initialization: $n = 1$ (the first iteration). A column of vector x_j in the spectrum matrix is selected and labeled as $x_{k(0)}(k\,(0) = j)$.
2) The set S is defined as $S = \{j, 1 \le j \le K, j \notin \{k(0), \ldots, k(n-1)\}\}$. The column vectors that have not been selected into the wavelength chain were calculated as the projection vector x_j in S

$$Px_j = x_j - (x_j^T - x_{k(n-1)}) \times x_{k(n-1)}(x_{k(n-1)}^T - x_{k(n-1)})^{-1}. \quad (6)$$

3) The number of the largest projection of recorded

$$k(n) = arg(max||Px_j||, j \in S). \quad (7)$$

4) The maximum projection is used as the projection vector in the next round

$$x_j = Px_j, j \in S. \quad (8)$$

5) $n = n + 1$: if $n < N$, repeat step 2) to continue projection.

After this process, N^*K pairs of wavelength combinations are obtained, a calibration model is established for each combination determined by $x_{k(0)}$ and N, and the root-mean-square error of prediction (RMSEP) is used to determine the established model. The smallest RMSEP is chosen, and its corresponding $x^*_{k(0)}$ and N^* are considered the best wavelength combinations.

D. Contribution Value Selection

Analyzing the principle of the SPA, it can be seen that the SPA calculates the projection of a certain wavelength in the absorbance matrix to other wavelengths and selects the wavelength with the greatest projection as the next wavelength in the wavelength sequence. Each wavelength in the sequence has the lowest correlation with the previous wavelength, which eliminates the influence of collinearity on the model to the greatest extent and reduces the model complexity.

Since the selection of each sequence in the projection process does not consider the information of the component to be measured, this will lead to the selection of a wavelength sequence that is not sensitive to the component. To further reduce the complexity of the model, the wavelength that does not contribute much to the component to be measured is eliminated. In this study, the SPA is used as the independent variable, and the depth of the Qinghai Lake water body is used as the dependent variable to construct a multivariate monitoring model (SPA-MLM) to estimate the water depth of Qinghai Lake

$$\hat{y} = b_0 + b_1 x_1 + b_2 x_2 + \cdots + b_L x_L. \quad (9)$$

Its residual square and Q_{total} is calculated as follows:

$$Q_{\text{total}} = \sum_{i=1}^{n} (y_i - \hat{y})^2. \quad (10)$$

The sum of residual squares for the new model is calculated separately each time one wavelength is removed to participate in the establishment of the model, which is recorded as

$Q_1, Q_2, \ldots, Q_L$. Therefore, the contribution value corresponding to each wavelength can be obtained as

$$C_i = (Q_i - Q_{\text{total}})/Q_{\text{total}}, \quad i = 1, \ldots, L \tag{11}$$

where C_i and Q_i are the contribution value and the residual square for band i, respectively.

The wavelengths are reordered according to the magnitude of the contribution value, the wavelength with the smallest contribution value in the sequence is sequentially eliminated, and a new multiple regression model is established. When the prediction accuracy of the built model is greatly reduced (F-test with a significance level of 0.25 as the standard), elimination is terminated.

E. Model Validation and Evaluation

The predictive performance of the model established by the SPA-MLM is mainly judged by the square of the correlation coefficient (R^2) and the RMSE between the measured value and the predicted value of the datasets. The closer the R^2 value of the model is to 1 and the smaller the RMSE, the better the prediction performance of the model and the higher the prediction accuracy will be. This study mainly uses the R^2 and RMSEP set samples as the main criteria.

The calculation formula of R^2 is as follows:

$$R^2 = \left(\frac{\sum_{i=1}^{n} (x_i - \overline{x})(y_i - \overline{y})}{\sqrt{\sum_{i=1}^{n} (x_i - \overline{x})^2} \sqrt{\sum_{i=1}^{n} (y_i - \overline{y})^2}} \right)^2 \tag{12}$$

where x_i is the measured value of sample i, $\bar{x}$ is the average value, y_i is the predicted value of sample i, $\bar{y}$ is the average value of y, and n is the number of samples.

The RMSE equation is as follows:

$$\text{RMSE} = \sqrt{\frac{1}{n} \sum_{i=1}^{n} (y_i - y_p)^2} \tag{13}$$

where y_i is the measured value of sample i and y_p is the predicted value of sample i.

III. Study Area and Data

A. Study Area

The Qinghai Lake is the largest inland saltwater lake in China. It is located in the northeastern part of the Qinghai–Tibet Plateau (36°32'∼37°15'N, 99°36'∼100°46'E) across the three counties of Gangcha, Haiyan, and Gonghe in Qinghai Province, with a length of approximately 109 km from east to west. It is approximately 40 km wide from north to south (see Fig. 3). According to the 2013 measurement data released by the first water conservancy survey in Qinghai Province, the Qinghai Lake area is 4337.48 km^2, the water volume is 73.9 billion m^3, the longest point is approximately 104 km long, the widest point is approximately 62 km wide, and the maximum water depth is 31.4 m [42]. The main types of vegetation in the Qinghai Lake Basin are high mountain, subalpine meadow, grassland, wetland, and shrub species. The lake is located at the intersection of the monsoon zone in eastern China, the arid zone in the northwest, and the alpine zone in the southwest. It has a typical plateau semi-arid and alpine climate [43]. However, due to climate change and intensified human activities, the cultivated area is increasing, and the land has been desertified, which has led to the deterioration of the ecological environment, thereby increasing eutrophication and the degree of serious water pollution in the Qinghai Lake Basin. The implementation of environmental protection in the Qinghai Lake Basin is becoming increasingly urgent.

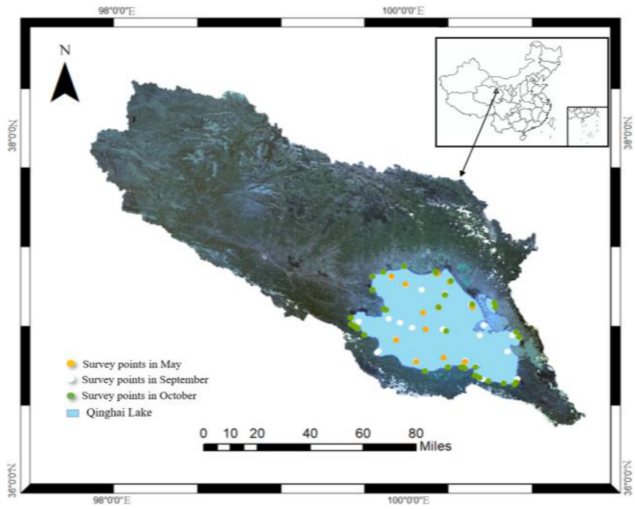

Fig. 3. Study area and survey points for water depth.

B. Remote Sensing Data

The satellite data used in this study all came from the "Zhuhai-1" hyperspectral satellite (OHS). It is the second group of satellites in the Zhuhai-1 satellite constellation. It was launched successfully from the Jiuquan Satellite Launch Center on April 26, 2018 by the Long March rocket and has been in continuous use since at [44]. The size of the satellite is approximately 600 mm × 600 mm × 800 mm, its weight is 71 kg, and its designed orbit life is five years. A single hyperspectral satellite can orbit the Earth approximately 15 or 16 times a day, and the acquisition time for a single data point per orbit does not exceed 8 min. At present, the revisit period of a single satellite is six days, and the revisit period of four satellites has been shortened to two days.

In this study, the high-quality image was used to retrieve the water depth in Qinghai Lake that acquired on September 25, 2020. It has a spatial resolution of 10 m and a spectral resolution of about 2.5 nm, and a wavelength range of 400–1000 nm. Due to compression and storage limitations, the system is designed to transmit 32 bands. The main performance indicators of the satellite are presented in Table I.

C. In Situ Measured Water Depth Data

In this study, an SZ-SFCC hand-held ultrasonic sounder[1] is used for water depth measurement. Ultrasonic sounding is one

[1][Online]. Available: http://www.shshuozhou.com/showpro.asp?id = 449

TABLE I
OHS HYPERSPECTRAL SATELLITE ORBIT AND SENSOR TECHNICAL PARAMETERS

Item		Parameters
Orbit	Type	Sun-synchronous orbit
	Inclination	98°
	Altitude	500km
Lifespan	lifespan	5 years
Hyperspectral Imager	Imaging	Push-broom imaging
	Spatial resolution	< 10m
	Spectral resolution	2.5nm
	Width	150km
	Signal-to-noise ratio	< 300
	Wavelength No.	>32
	Spectral range	400nm - 1000nm

Fig. 4. Distribution of the *in situ* water depth measurements for 98 sites.

of the commonly used methods to measure water depth. It is able to collect multiple, real-time observation measurements, with high precision. The water depth was measured using the boat from the Qinghai Lake Scenic Area Administration Scientific Research. When installing the sensor, the end face of the ultrasonic sensor was made perpendicular to the lake surface, and the probe was reached 20 cm deep into the lake surface (the error can be adjusted and eliminated in the sensor measurement setting). Meanwhile, the geographic coordinates of the sample points were recorded through the handheld GPS receiver. The water depth is measured three times for each sampling point. To eliminate errors caused by improper operation and other reasons, a total of 98 sampling points and 294 water depth data were obtained. When the laboratory processes the data, the data of each sampling point are averaged to obtain the ultrasonic depth data of Qinghai Lake. The sonar working frequency is 200-2000 kHz that can be selected arbitrarily. The minimum display resolution is about 1 mm and the maximum error is approximately 0.3% of the range. In order to effectively remove various interferences (such as environmental noise interference and low-frequency electrical noise), a bandpass filter with a center frequency of 300 kHz was inserted as an antialiasing filter. The *in situ* measured water depth data were obtained from three field acquisition voyages in Qinghai Lake in May, September, and October 2020. There are 98 sampling points that basically cover the whole Qinghai Lake area and the distribution of the *in situ* water depth measurements is shown in Fig. 4.

IV. RESULTS AND DISCUSSION

A. Sensitive Band Selection and Comparison of Different Bathymetry Retrieval Models

Several common methods have been developed in the research of water depth retrieval, such as the single-band method, two-band method (ratio, difference), and three-band method. The single-band method mainly uses correlation to select the sensitive band with the largest correlation coefficients and then uses the least squares method to establish a function to retrieve the water depth. Similar to the mechanism of the single-band method, the optimal mathematical relationship between the two bands and the actual water depth can be established by selecting the two sensitive bands with the largest correlation coefficient. The ratio and difference processes were always calculated through the mathematical operations of the two bands. This process is improved in this study, and the normalized ratio model is constructed to obtain the inversed water depth. By selecting the three most sensitive bands, the three-band model constructs the correlation exponential model to retrieve the water depth.

To choose the most sensitive band to estimate the water depth, a correlation analysis was performed on the reflectance of 400–1000 nm and the water depth to obtain the square correlation coefficient (R^2) (see Fig. 5). The reflectivity and water depth mainly show a negative correlation trend, which is in line with the general rule that the emitted radiance of the water body attenuates as the water depth increases. Among them, the maximum correlation coefficient was at 596 nm ($R^2 = 0.78$). The band ratio can eliminate the influence of the background to a certain extent. The ratio is calculated according to the reflectance of the different combinations of various bands, and then a correlation analysis is carried out with the water depth. The results show that the ratio between B28 and B22 is the most sensitive variable to water depth, and the correlation coefficient is 0.70. Using this ratio as a factor, the water depth band ratio model is established based on the least squares method. Moreover, the band difference method is applied to establish the water depth retrieval model. Similar to the ratio method, a correlation analysis is carried out with the water depth. The difference between B13 and B10 is the most sensitive variable to the water depth, and the correlation coefficient is 0.67. Using the SPA to select the best bands for Zhuhai-1 hyperspectral remote sensing images, the parameters were set, and the selected bands were obtained. The sensitive bands for water depth refer to six bands [as shown in Fig. 5(b)], which are located at 566, 596, 656, 820, 536, and 466 nm. Compared with the total spectral information, the selected three bands can represent approximately 90% of all the bands. Therefore, three bands were chosen to establish the water depth retrieval model in this study. There are many water

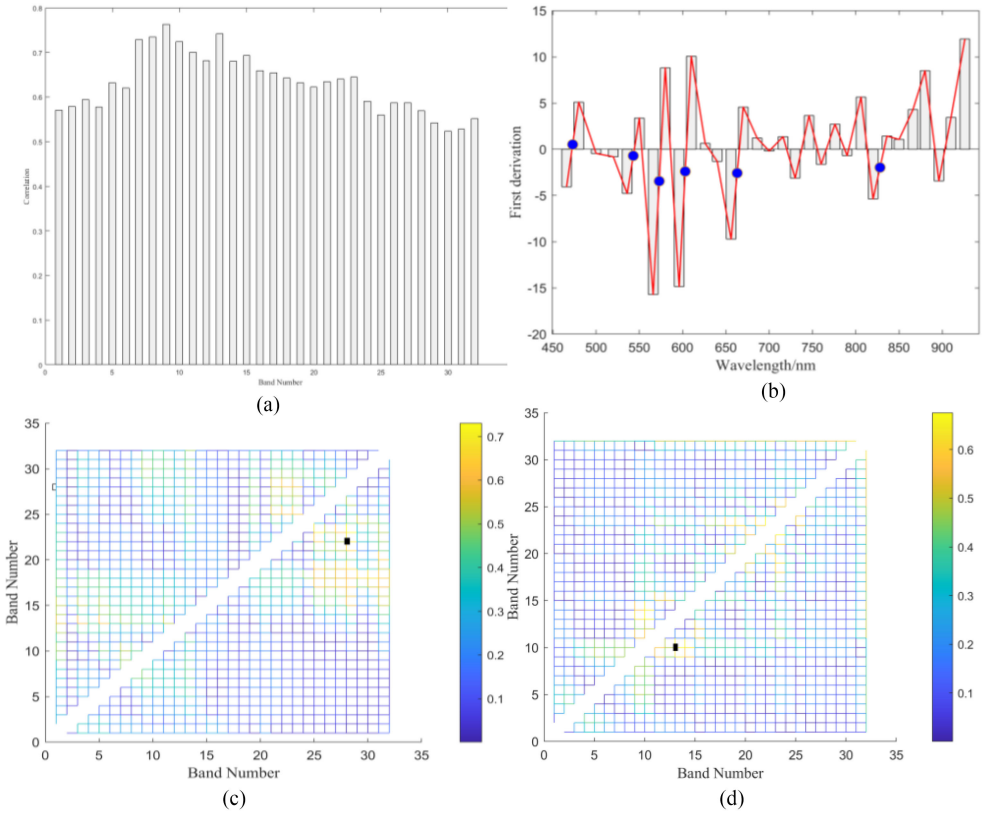

Fig. 5. Best sensitive bands selection for different methods. (a) Single-band method. (b) SPA method. (c) Ratio method. (d) Difference method. The blue circles in (b) show the six best sensitive bands selected by SPA method. The black squares in (c) and (d) represent the best band combinations for ratio method and difference method.

TABLE II
DATASETS FOR MODEL ESTABLISHMENT AND VALIDATION

Data sets	No.	Minimum (m)	Maximum (m)	Average (m)	RMSE (m)
Total data	98	0.56	29.36	19.40	1.35
Modeling	66	0.56	29.36	19.20	1.29
Validation	32	0.63	28.71	19.86	1.26

depth-sensitive bands selected by the SPA algorithm, which can be used for modeling. With the addition of band numbers, the retrieval accuracy is improved, but the level is not large, which will make the retrieval model more complex and less applicable. Therefore, in this study, the water depth retrieval model is established by using the three selected optimal bands, which can not only ensure higher accuracy but also reduce the complexity of the model.

In this study, the *in situ* measured water depth data were divided into two parts: one part was selected to establish the retrieval model. The other part was retained for validation. Therefore, the total number of *in situ* measurements is 98. In all, 66 points were input for model establishment, and 32 points were reserved for validating the estimation results (as presented in Table II).

To validate the universal application of the established bathymetry estimation model in this study, it is compared with the commonly used single-band, double-band (ratio, difference), and three-band models, and the same dataset is used for modeling and verification. The comparison results are presented in Table III. The correlation coefficients of the single-band and two-band models are lower, which is more suitable for water depth retrieval from multispectral images. It is mainly affected by the few available bands of the multispectral remote sensors or poor spectral quality. The correlation coefficients of the ratio model and difference model are slightly higher than those of the single-band and two-band methods, but they use little spectral information. For hyperspectral images, more spectral information can be used for water depth retrieval. The three-band model can use more spectral information for model establishment and retrieve the water depth more accurately. Although more bands participating in the modeling slightly improve the accuracy relative to the three-band model, the improvement is not large, and the complexity is much larger than that of the three-band model. From the perspective of comprehensive optimization, the three-band model has the highest cost performance.

The different bathymetry estimation models and their validation using the two datasets are shown in Fig. 6. The single-band optimal wavelength is at B9, and the wavelength is 596 nm. The correlation coefficient is 0.71, and the RMSE is 1.57 m for the modeling dataset. The correlation coefficient is 0.74, and

TABLE III
COMPARISON OF DIFFERENT WATER DEPTH RETRIEVAL MODELS BASED ON REMOTE SENSING DATA

Method	Models	Modeling R^2	Validation R^2	RMSE (m)
B9	y = -1453.5x + 32.36	0.52	0.56	2.18
B28/B22	y = -43.67x + 47.40	0.71	0.74	1.64
B28-B22	y = -3079.7x + 27.75	0.55	0.52	2.43
B28/(B9+B22)	y = -50.05x + 35.01	0.76	0.76	1.35
(B28-B22-B9)/(B28+B22-B9)	y = -37.17x – 3.39	0.75	0.83	1.29
SPA-MLM	y=30.45-721.09*B28-336.33*B9 -421.01*B13	0.85	0.92	1.26

the RMSE is 1.64 m for the validation dataset. The accuracy error of the single-band model for shallow water depths is large, and the fitting effect of shallow water depths is poor, as shown in the right figure. The best wavelength of the ratio model is B22 and B28, and the wavelength is 790 and 880 nm. The correlation coefficient is 0.52, and the RMSE is 3.26 m for the modeling dataset. The correlation coefficient is 0.56, and the RMSE is 1.64 m for the validation dataset. The accuracy error of the ratio model is larger than that of the other methods. Based on the difference model, the optimal wavelengths are B10 and B13, and the wavelength is 610 nm and 656 nm. The correlation coefficient is 0.55, and the RMSE is 3.29 m for the modeling dataset. The correlation coefficient is 0.52, and the RMSE is 2.43 m for the validation dataset. Compared with several models, we can see that the difference model performs the worst. The optimal wavelength of the dual-band ratio model is located at B22 and B28, which is the same as the ratio model. The correlation coefficient is 0.76, and the RMSE is 1.32 m for the modeling dataset. The correlation coefficient is 0.76, and the RMSE is 1.25 m for the validation dataset. The two-band ratio model is more robust than the previous three models, and the depth retrieval accuracy is higher. The optimal wavelengths of the three-band ratio model are B9, B22, and B28. The correlation coefficient is 0.75, and the RMSE is 1.35 m for the modeling dataset. The correlation coefficient is 0.83, and the RMSE is 1.35 m for the validation dataset. The three-band ratio model has a high accuracy in depth retrieval. The optimal wavelength of SPA-MLM is B9, B13, and B28. The correlation coefficient is 0.85, and the RMSE is 1.48 m for the modeling dataset. The correlation coefficient is 0.92, and the RMSE is 1.26 m for the validation dataset. The SPA-MLM method can be used to retrieve the water depth over the Qinghai Lake area with a high accuracy exceeding 90%.

Through comparative analysis, it was demonstrated that the SPA-MLM model can select the best spectral bands among many hyperspectral bands, and then a water depth retrieval model was built combined with the measured water depth modeling set and verified the predicted water depth through the verification set. The results showed that the SPA-MLM method can better retrieve the water depth of Qinghai Lake, which has a higher retrieval accuracy than other methods. It also shows that the method selected in this study is feasible to retrieve the water depth in the Qinghai Lake area.

B. Bathymetry Retrieval Model Establishment

The dataset was used to establish the water depth retrieval model and applied to the study area. The shallowest water depth in the dataset is 0.56 m, the maximum water depth is 29.36 m, and the average water depth is 19.40 m. For the data modeling set, the minimum water depth in the total dataset is 0.56 m, the maximum water depth is 29.36 m, and the average water depth is 19.20 m. For the data validation set, the minimum water depth in the dataset is 0.63 m, the maximum water depth is 28.71 m, and the average water depth is 19.86 m. The RMSEs for these three datasets were 1.35, 1.29, and 1.26 m, respectively. The water depth retrieval model is established using multiband regression as follows:

$$D = 30.45 - 721.09 \times B28 - 336.33 \times B9 - 421.01 \times B13 \tag{14}$$

where D is the retrieval water depth and B9, B13, and B28 are the reflectivities of the three selected optimal sensitive bands.

The water depth in Qinghai Lake was obtained using the established model (14), as shown in Fig. 7. Through comprehensive analysis, the correlation coefficient is 0.85, and the RMSE is 1.48 m for the modeling dataset. The established water depth model is applied to the measured validation set, the correlation coefficient is 0.92, and the RMSE is 1.26 m, which shows that the established water depth model can accurately invert the water depth of Qinghai Lake. By analyzing the spatial distribution of water depth, it can be concluded that the water depth of Qinghai Lake is higher to the west and lower to the east. The water depth in the middle is deeper, with an average depth of 24 m. The average water depth in the west is deeper than that in the east. According to previous studies, the water depth of Qinghai Lake can be divided into three areas: a deep water area, a shallow water area, and a middle area. The retrieval results of the hyperspectral remote sensing imagery are consistent with the results of previous studies, which further shows that the use of remote sensing image retrieval of water depth is feasible and has the advantages of large-scale and rapid periodic monitoring, which can provide support for environmental monitoring departments.

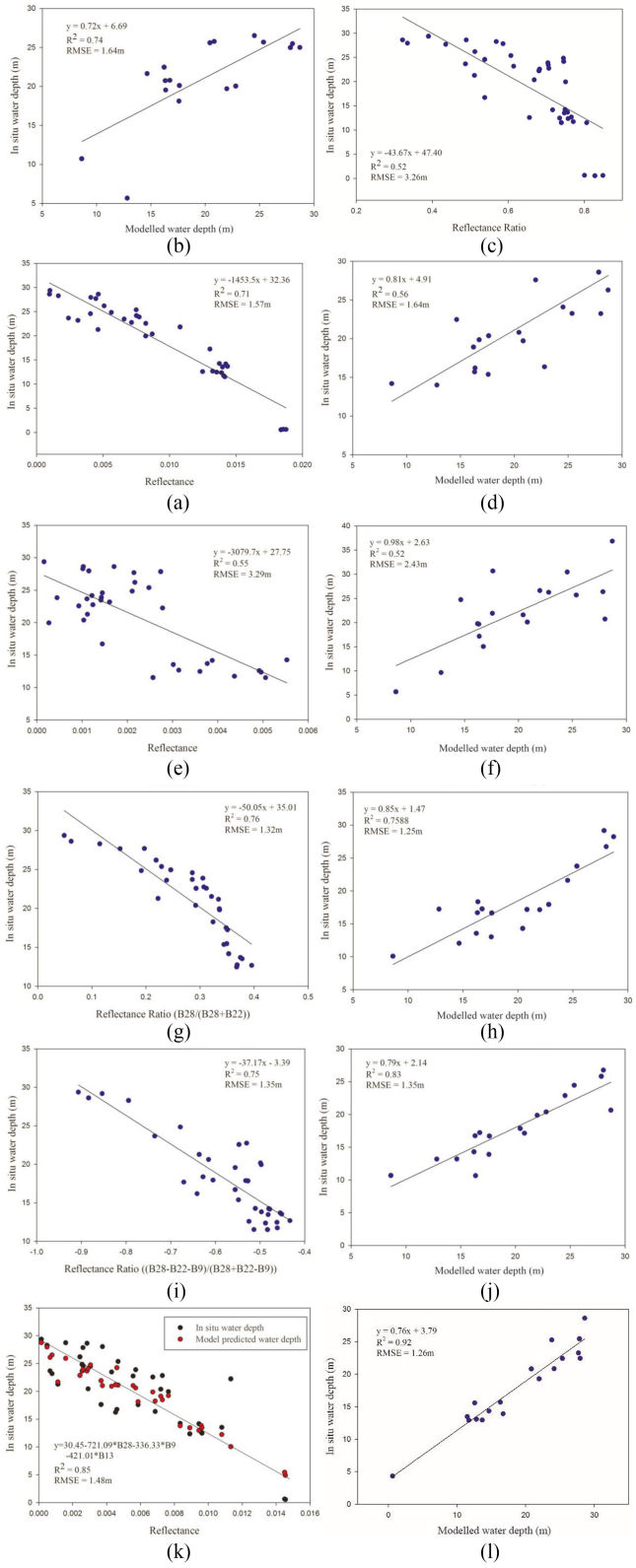

Fig. 6. Results of different water depth retrieval models using the same dataset. The left figures [(a), (c), (e), (g), (i), (k)] show the modeling dataset and the right figures [(b), (d), (f), (h), (j), (l)] show the validation dataset. (a) and (b) are the results using single-band method; (c) and (d) are the results using band ratio method; (e) and (f) are the results using two-bands difference method; (g) and (h) are the results using two-bands ratio index method; (i) and (j) are the results using three bands ratio index method; (k) and (l) are the results using SPA-MLM method.

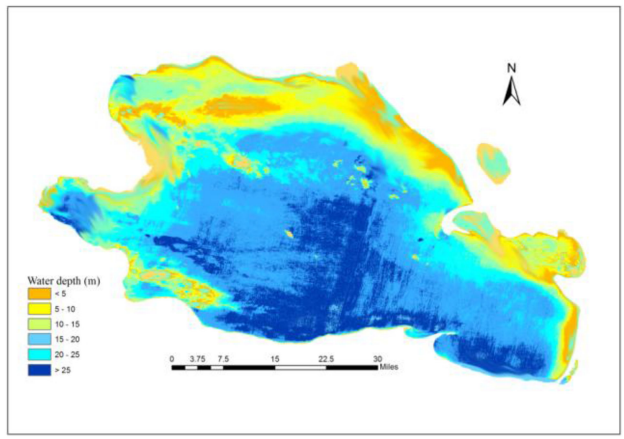

Fig. 7. Estimation bathymetry results in Qinghai Lake using ZH-1 hyperspectral remote sensing data on September 2020.

C. Discussion

The reflectance of the water body comes from the radiated energy directly reflected from the water surface, the backscattered radiation energy of the water body, and the reflected radiation energy from the bottom. The results demonstrated that the application of the single-band model and band ratio model for water depth remote sensing retrieval is restricted by certain preconditions, and the retrieval accuracy of water areas with large differences in the sediment composition and water quality is affected. The SPA-MLM model can eliminate the influence of the linear background signal and eliminate some errors caused by uneven water quality, especially the backscattered energy of suspended sediment in the study area. The water depth resolution of visible light remote sensing depends on the attenuation coefficient of the water body. The larger the attenuation coefficient is, the faster the attenuation and the greater the water depth resolution. The longwave band has a large attenuation coefficient on the water body, so the resolution of the water depth change is high, and the amount of carried water depth information is greater.

This study confirmed that hyperspectral remote sensing images can be used to accurately retrieve water depth, but in the SPA-MLM modeling process, they are combined with the measured water depth data for multiband fitting analysis. The optimal fitting equation was selected as the water depth retrieval model. This process lacks a robust physical basis and introduces certain errors in the process of statistical fitting. Moreover, the advantage of hyperspectral data lies in high-precision spectral data and rich spectral information. In this study, only three sensitive bands were selected when using SPA method for water depth modeling. The used spectral information was less, and it was difficult to display rich hyperspectral information. Compared with single-band, dual-band, and three-band algorithms, although the SPA method can extract effective sensitive bands and increase the accuracy of water depth retrieval, the physical mechanism of spectral transmission in water is less used in this process, which makes it difficult to form a universal depth retrieval algorithm. From the analysis of the inverted water depth, it can be seen that

the error of water depth retrieval using remote sensing technology is slightly larger than that of other instruments, and further improvement is required in engineering applications. Combined with the advantages of remote sensing for large-area, rapid, periodic monitoring, the water depth retrieval model can be better established by matching the corresponding aerial remote sensing and ground spectral measurements, which is a solid step toward practical development.

Through the comparative analysis of various bathymetry retrieval models, it can be seen that each model has its own applicability and assumptions, which provide a reference for the use of different data sources for various purposes. Under the premise of an improved data quality, all kinds of models can obtain satisfactory retrieval results. Therefore, it is very important to select a suitable retrieval model for water depth retrieval.

V. Conclusion

This study aims to estimate water depth using hyperspectral remote sensing data collected over Qinghai Lake. A multiband retrieval model was developed based on a SPA for sensitive band selection. Through comparison with the other traditional methods, it is determined that the established model in this study has a better water depth retrieval accuracy in Qinghai Lake. *In situ* measurements of water depth were applied to validate the estimation results. This result demonstrated that the related coefficient of the retrieval and *in situ* water depth reached approximately 0.92, and the RMSE was approximately 1.26 m. The retrieval accuracy was high, which showed that the model was applicable in the study area.

Moreover, the other traditional water depth models were evaluated using *in situ* measurements. The single-band method and two-band method obtained poor retrieval results in that they have exhibit a poor relationship between the estimated values and *in situ* measurements. This is mainly due to the lower amount of spectral information used in these two models or because the selected spectral bands cannot represent a majority of the spectral information. The three-band method can achieve a higher retrieval accuracy than the above-mentioned methods. However, the three selected bands rely on the relationship between the water depth and reflectance, which is not robust on a physical basis. Overall, the model proposed in this study can not only accurately estimate the water depth but also has a certain supporting physical mechanism.

Water depth estimation by remote sensing technology is a challenging task due to the complexity of radiation transmission. The effect of the atmosphere and the interaction between the air and water surface are the principal factors that should be eliminated in water depth retrieval. In addition, the development of bathymetric retrieval models supported by physical mechanisms should be the development direction in the future.

References

[1] Y. Dong, Y. Liu, C. Hu, and B. Xu, "Coral reef geomorphology of the Spratly Islands: A simple method based on time-series of Landsat-8 multiband inundation maps," *ISPRS J. Photogramm. Remote Sens.*, vol. 157, pp. 137–154, 2019.

[2] T. Kutser, J. Hedley, C. Giardino, C. Roelfsema, and V. E. Brando, "Remote sensing of shallow waters—A 50 year retrospective and future directions," *Remote Sens. Environ.*, vol. 240, 2020, Art. no. 111619.

[3] R. J. Nicholls and A. Cazenave, "Sea-level rise and its impact on coastal zones," *Science*, vol. 328, no. 5985, pp. 1517–1520, 2010.

[4] Y. Ma *et al.*, "Satellite-derived bathymetry using the ICESat-2 LiDAR and Sentinel-2 imagery datasets," *Remote Sens. Environ.*, vol. 250, 2020, Art. no. 112047.

[5] C. Cahalane, A. Magee, X. Monteys, G. Casal, J. Hanafin, and P. Harris, "A comparison of Landsat 8, RapidEye and Pleiades products for improving empirical predictions of satellite-derived bathymetry," *Remote Sens. Environ.*, vol. 233, 2019, Art. no. 111414.

[6] Z. Lee, K. L. Carder, C. D. Mobley, R. G. Steward, and J. S. Patch, "Hyperspectral remote sensing for shallow waters. I. A semianalytical model," *Appl. Opt.*, vol. 37, no. 27, pp. 6329–6338, 1998.

[7] F. Yang, X. Bu, Y. Ma, X. Lu, M. Wang, and B. Shi, "Geometric calibration of multibeam bathymetric data using an improved sound velocity model and laser tie points for BoMMS," *Ocean Eng.*, vol. 145, pp. 230–236, 2017.

[8] P. Westfeld *et al.*, "Analysis and correction of ocean wave pattern induced systematic coordinate errors in airborne LiDAR bathymetry," *ISPRS J. Photogramm. Remote Sens.*, vol. 128, pp. 314–325, 2017.

[9] J. Gao, "Bathymetric mapping by means of remote sensing: Methods, accuracy and limitations," *Prog. Phys. Geography*, vol. 33, no. 1, pp. 103–116, 2009.

[10] Z. Lee, K. L. Carder, C. D. Mobley, R. G. Steward, and J. S. Patch, "Hyperspectral remote sensing for shallow waters: 2. Deriving bottom depths and water properties by optimization," *Appl. Opt.*, vol. 38, no. 18, pp. 3831–3843, 1999.

[11] D. R. Lyzenga, "Remote sensing of bottom reflectance and water attenuation parameters in shallow water using aircraft and Landsat data," *Int. J. Remote Sens.*, vol. 2, no. 1, pp. 71–82, 1981.

[12] P. Chernyshov, T. Vrecica, and M. Streßer, "Rapid wavelet-based bathymetry inversion method for nearshore X-band radars," *Remote Sens. Environ.*, vol. 240, 2020, Art. no. 111688.

[13] J. Wei, M. Wang, and Z. Lee, "Shallow water bathymetry with multispectral satellite ocean color sensors: Leveraging temporal variation in image data," *Remote Sens. Environ.*, vol. 250, 2020, Art. no. 112035.

[14] R. P. Stumpf, K. Holderied, and M. Sinclair, "Determination of water depth with high-resolution satellite imagery over variable bottom types," *Limnol. Oceanogr.*, vol. 48, no. 1, pp. 547–556, 2003.

[15] A. G. Dekker *et al.*, "Intercomparison of shallow water bathymetry, hydro-optics, and benthos mapping techniques in Australian and Caribbean coastal environments," *Limnol. Oceanogr. Methods.*, vol. 9, no. 9, pp. 396–425, 2011.

[16] B. Barnes, R. Garcia, C. Hu, and Z. Lee, "Multi-band spectral matching inversion algorithm to derive water column properties in optically shallow waters: An optimization of parameterization," *Remote Sens. Environ.*, vol. 204, pp. 424–438, 2018.

[17] A. Mateo-Sanchis, M. Piles, and J. Muoz-Marí, "Synergistic integration of optical and microwave satellite data for crop yield estimation," *Remote Sens. Environ.*, vol. 234, 2019, Art. no. 111460.

[18] M. Gholamalifard, A. Sari, and A. Abkar, "Bathymetric modeling from satellite imagery via single band algorithm (SBA) and principal components analysis (PCA) in southern Caspian Sea," *Int. J. Environ. Res.*, vol. 7, pp. 877–886, 2013.

[19] C. E. Parrish, L. A. Magruder, A. L. Neuenschwander, N. Forfinski-Sarkozi, M. Alonzo, and M. Jasinski, "Validation of ICESat-2 ATLAS bathymetry and analysis of ATLAS's bathymetric mapping performance," *Remote Sens.*, vol. 11, no. 14, 2019, Art. no. 1634.

[20] C. D. Mobley *et al.*, "Interpretation of hyperspectral remote-sensing imagery by spectrum matching and look-up tables," *Appl. Opt.*, vol. 44, no. 17, pp. 3576–3592, 2005.

[21] L. Zhang *et al.*, "Bathymetry using hyperspectral imagery based on semi-analytical model," *Hydrographic Surveying Charting*, vol. 31, no. 4, pp. 17–21, 2011

[22] G. Casal, X. Monteys, J. Hedley, P. Harris, C. Cahalane, and T. McCarthy, "Assessment of empirical algorithms for bathymetry extraction using Sentinel-2 data," *Int. J. Remote Sens.*, vol. 40, no. 8, pp. 2855–2879, 2019.

[23] G. Casal, J. D. Hedley, X. Monteys, P. Harris, C. Cahalane, and T. McCarthy, "Satellite-derived bathymetry in optically complex waters using a model inversion approach and Sentinel-2 data," *Estuarine Coastal Shelf Sci.*, vol. 241, 2020, Art. no. 106814.

[24] X. Monteys, P. Harris, S. Caloca, and C. Cahalane, "Spatial prediction of coastal bathymetry based on multispectral satellite imagery and multibeam data," *Remote Sens.*, vol. 7, no. 10, pp. 13782–13806, 2015.
[25] J. C. Sandidge and R. J. Holyer, "Coastal bathymetry from hyperspectral observations of water radiance," *Remote Sens. Environ.*, vol. 65, no. 3, pp. 341–352, 1998.
[26] Y. N. Shi, "Study of the hyperspectral remote sensing of shallow waters bathymetry with artificial neural network technology," Ocean Univ. China, Qingdao, China, 2005.
[27] Z. Lee, K. L. Carder, R. F. Chen, and T. G. Peacock, "Properties of the water column and bottom derived from airborne visible infrared imaging spectrometer (AVIRIS) data," *J. Geophys. Res., Oceans*, vol. 106, no. C6, pp. 11639–11651, 2001.
[28] Z. Lee *et al.*, "Water and bottom properties of a coastal environment derived from hyperion data measured from the EO-1 spacecraft platform," *J. Appl. Remote Sens.*, vol. 1, no. 1, 2007, Art. no. 011502.
[29] F. Liu, "Fast and nondestructive detection of Brassica napus growth information using spectral and multi-spectral imaging technology," Zhejiang Univ., Hangzhou, China, 2011.
[30] I.-G. Chong and C.-H. Jun, "Performance of some variable selection methods when multicollinearity is present," *Chemom. Intell. Lab. Syst.*, vol. 78, no. 1/2, pp. 103–112, 2005.
[31] F. Liu, Y. He, and L. Wang, "Comparison of calibrations for the determination of soluble solids content and pH of rice vinegars using visible and short-wave near infrared spectroscopy," *Anal. Chim. Acta*, vol. 610, no. 2, pp. 196–204, 2008.
[32] K. H. Esbensen, *Multivariate Data Analysis: In Practice*. Oslo, Norway: CAMO, 2002.
[33] F. Liu, Y. He, L. Wang, and H. Pan, "Feasibility of the use of visible and near infrared spectroscopy to assess soluble solids content and pH of rice wines," *J. Food Eng.*, vol. 83, no. 3, pp. 430–435, 2007.
[34] A. Hyvärinen and E. Oja, "Independent component analysis: Algorithms and applications," *Neural Netw.*, vol. 13, no. 4/5, pp. 411–430, 2000.
[35] J. V. Stone, "Independent component analysis: An introduction," *Trends Cogn. Sci.*, vol. 6, no. 2, pp. 59–64, 2002.
[36] A. Huete, H. Liu, K. Batchily, and W. Van Leeuwen, "A comparison of vegetation indices over a global set of TM images for EOS-MODIS," *Remote Sens. Environ.*, vol. 59, no. 3, pp. 440–451, 1997.
[37] J. Chen and X. Wang, "A new approach to near-infrared spectral data analysis using independent component analysis," *J. Chem. Inf. Model.*, vol. 41, no. 4, pp. 992–1001, 2001.
[38] M. C. U. Araújo, T. C. B. Saldanha, R. K. H. Galvao, T. Yoneyama, H. C. Chame, and V. Visani, "The successive projections algorithm for variable selection in spectroscopic multicomponent analysis," *Chemom. Intell. Lab. Syst.*, vol. 57, no. 2, pp. 65–73, 2001.
[39] L. Galvao, I. Vitorello, and M. Pizarro, "An adequate band positioning to enhance NDVI contrasts among green vegetation, senescent biomass, and tropical soils," *Int. J. Remote Sens.*, vol. 21, no. 9, pp. 1953–1960, 2000.
[40] M. Niroumand-Jadidi, A. Vitti, and D. R. Lyzenga, "Multiple optimal depth predictors analysis (MODPA) for river bathymetry: Findings from spectroradiometry, simulations, and satellite imagery," *Remote Sens. Environ.*, vol. 218, pp. 132–147, 2018.
[41] E. Kasvi, J. Salmela, E. Lotsari, T. Kumpula, and S. Lane, "Comparison of remote sensing based approaches for mapping bathymetry of shallow, clear water rivers," *Geomorphology*, vol. 333, pp. 180–197, 2019.
[42] Qinghai Provincial Water Resources Department, Qinghai Provincial Bureau of Statistics, "The first water resources census bulletin of Qinghai province," *Qinghai Statist.*, vol. 28, no. 4, pp. 34–39, 2015.
[43] Y. Mo-Juan, L. Xiao-Yan, C. Bu-Li, and M. Yo-Jun, "Climate change and impact on water level of the Qinghai Lake watershed," *J. Arid Meteorol.*, vol. 28, no. 4, pp. 375–383, 2010.
[44] X. Li and H. Fan, "Overview of Zhuhai-1 hyperspectral satellite data and application," *Satell. Appl.*, no. 8, pp. 12–18, 2019.

Dianjun Zhang was born in Shandong, China, in 1986. He received the M.S. degree in geographical information system from Beijing Forestry University, Beijing, China, in 2011, and the Ph.D. degree in geographical information system from the Institute of Geographic Sciences and Natural Resources Research, Chinese Academy of Sciences, Beijing, China, in 2015.

His research interests include ocean remote sensing and ship recognition based on deep learning methods.

Quan Guo was born in Jiangxi, China, in 1998. He received the B.S. degree in marine technology, School of Marine Science and Technology, Tianjin University, China, in 2020. He is currently pursuing the M.S. degree in marine technology, School of Marine Science and Technology, Tianjin University. His research interest is the inversion of the three-dimensional temperature field using ocean remote sensing methods.

Lingjuan Cao was born in Zhejiang, China, in 1997. She received the B.S. degree in marine technology, North China University of Science and Technology, China, in 2020. She is currently pursuing the M.S. degree in marine technology, School of Marine Science and Technology, Tianjin University. Her research interest is ocean mesoscale eddies with remote sensing.

Guoqing Zhou (Senior Member, IEEE) received the Ph.D. degree in photogrammetry and remote sensing from Wuhan University, Wuhan, China, in 1994.

He was a Visiting Scholar with the Department of Computer Science and Technology, Tsinghua University, Beijing, China, and a Postdoctoral Researcher with the Institute of Information Science, Beijing Jiaotong University, Beijing, China. He continued his research as an Alexander von Humboldt Fellow with the Technical University of Berlin, Berlin, Germany, from 1996 to 1998, and was a Postdoctoral Researcher with The Ohio State University, Columbus, OH, USA, from 1998 to 2000. He was an Assistant Professor, Associate Professor, and Full Professor with Old Dominion University, Norfolk, VA, USA, in 2000, 2005, and 2010, respectively. He has authored five books and more than 380 refereed papers.

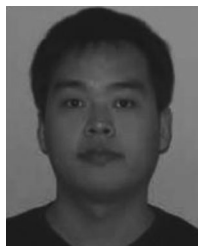

Guangyun Zhang received the B.Sc. degree in photogrammetry and remote sensing from the China University of Mining and Technology, Xuzhou, China, in 2007 and the Ph.D. degree in electrical engineering from the University of New South Wales, Sydney, Australia, in 2013.

Since 2019, he has been with the School of Geomatics Science and Technology, Nanjing Tech University, China, where he is currently a Professor. He is also with the University of New South Wales, Canberra, ACT, Australia. His research interests include imaging spectrometry and LiDAR.

Jie Zhan was born in Yantai, Shandong, China, in 1997. She received the B.S. degree in geomatics engineering from Shandong University of science and technology, Qingdao, China, in 2019. She is currently pursuing the M.S. degree in marine technology, School of Marine Science and Technology, Tianjin University. Her research interests include ocean color remote sensing and inversion algorithms.